Supporting Information

Perylene-based covalent organic frameworks for acid vapour sensing

Laura Ascherl,[1] Emrys W. Evans,[2] Jeffrey Gorman,[2] Sarah Orsborne,[2] Derya Bessinger,[1] Thomas Bein,[1] Richard H. Friend,[2] Florian Auras*[2]

[1]Department of Chemistry and Center for NanoScience (CeNS), University of Munich (LMU), Butenandtstraße 5-13, 81377 Munich, Germany
[2]Cavendish Laboratory, University of Cambridge, Cambridge CB3 0HE, United Kingdom
*e-mail: fa355@cam.ac.uk

Table of contents

Abbreviations

BET	Brunauer-Emmett-Teller	ITO	indium tin oxide
Boc	*tert*-butyloxycarbonyl	MCA	chloroacetic acid
CF	chloroform	Ms	mesyl
cod	cyclooctadiene	NMR	nuclear magnetic resonance
dba	dibenzylideneacetone	PTFE	poly(tetrafluoroethylene)
DCA	dichloroacetic acid	PXRD	powder X-ray diffraction
DCM	dichloromethane	QSDFT	quenched solid density functional theory
DFT	density functional theory	Sphos	dicyclohexylphosphino-2',6'-dimethoxybiphenyl
DMF	*N*,*N*-dimethylformamide	TCA	trichloroacetic acid
DMSO	dimethyl sulfoxide	TFA	trifluoroacetic acid
eq.	equivalents	THF	tetrahydrofuran
GIWAXS	grazing-incidence wide angle X-ray scattering	Ts	tosyl

COF building blocks

$Per(NH_2)_4$	2,5,8,11-tetrakis(4-aminophenyl)perylene
$Py(NH_2)_4$	1,3,6,8-tetrakis(4-aminophenyl)pyrene
$4PE(NH_2)_4$	1,1,2,2-tetrakis(4-aminophenyl)ethene
$Tz(NH_2)_3$	1,3,5-tris(4-aminophenyl)triazine
$1P(CHO)_2$	terephthalaldehyde
$N(CHO)_2$	naphthalene-2,6-dicarbaldehyde
$Py(CHO)_2$	pyrene-2,7-dicarbaldehyde
$1P^{OH}(CHO)_2$	2,5-dihydroxybenzene-1,4-dicarbaldehyde
$TT(CHO)_2$	thieno[3,2-*b*]thiophene-2,5-dicarbaldehyde
$Py(CHO)_4$	1,3,6,8-tetrakis(4-formylphenyl)pyrene

A. Methods

Powder X-ray diffraction (PXRD) patterns were measured on a Bruker D8 Advance diffractometer equipped with a Cu K_α source (0.1 mm or 0.2 mm divergence slit, static air scatter screen) and a LynxEye XE detector. K_β radiation was attenuated with a 0.0125 mm Ni filter. The PXRD patterns of the perylene COFs were recorded in two separate measurements with the instrument optimized for the small angle and wide-angle regions, respectively. The resulting patterns were scaled for identical peak intensity in the 3-8° (2 theta) region.

2D **grazing-incidence wide angle X-ray scattering (GIWAXS)** data were recorded with an Anton Paar SAXSpace system equipped with a GeniX Cu K_α Microsource and a Dectris EIGER R 1M detector. The COF films were positioned at sample-detector distances of 135 mm or 200 mm with a tilt angle of 2.3°.

The **structure models of the COFs** were constructed using the Accelrys Materials Studio software package. For each COF the highest possible symmetry was applied, taking into account the rotation of the peripheral phenylenes versus the respective core unit. **Structure refinements** using the Pawley or Rietveld methods, respectively, were carried out as implemented in the Reflex module of Materials Studio. Pseudo-Voigt peak profiles were used, and peak asymmetry was corrected using the Finger-Cox-Jephcoat method. **Connolly surfaces** and accessible surfaces were generated using an N_2-sized probe (r = 0.184 nm) at a 0.025 nm grid interval.[1]

Nitrogen sorption isotherms were recorded with Quantachrome Autosorb 1 and Autosorb iQ instruments at 77 K. The samples were outgassed for 24 h at 120°C under high vacuum prior to the measurements. Pore size distributions were calculated using the QSDFT equilibrium model with a carbon kernel for cylindrical pores.

Nuclear magnetic resonance (NMR) spectra were recorded on Bruker Avance III HD spectrometers. Proton chemical shifts are expressed in parts per million (δ scale) and are calibrated using residual undeuterated solvent peaks as an internal reference ($CDCl_3$: 7.26, DMSO-d_6: 2.50). Data for ^{1}H NMR spectra are reported in the following way: chemical shift (δ ppm) (multiplicity, coupling constant, integration). Multiplicities are reported as follows: s = singlet, d = doublet, t = triplet, q = quartet, m = multiplet, br. = broad, or combinations thereof.

UV-Vis-NIR spectra were recorded in transmission geometry using a Perkin-Elmer Lambda 1050 spectrometer equipped with a 150 mm InGaAs integrating sphere. The COF films were placed inside a fused silica cuvette filled with the respective acid vapour, solvent, or acid solution. For the **acid vapour sensing experiments**, 1.0 µL of the respective acid was evaporated at room temperature inside a 4.2 mL fused silica cuvette. For the acid vapour concentration series, 1 µL of a stock solution containing the desired TFA concentration in THF was used instead of the pure acid. The cuvette was purged with nitrogen after each acid vapour measurement. The COF films were handled and measured in air. Anhydrous solvents were used for preparing the acid solutions (this is only important for the 4PE-TT COF; the other COFs are stable towards humidity even when protonated).

Infrared (IR) spectra were recorded on a Perkin-Elmer Spectrum One FT-IR spectrometer fitted with an attenuated total reflectance (ATR) accessory, with internal reference. Absorptions are quoted to the nearest cm^{-1} in wavenumbers. For recording spectra of the protonated COFs, solid samples were acidified by exposure to TFA vapour for 3 s prior to each measurement.

Photoluminescence (PL) spectra were recorded using an Andor Shamrock spectrometer equipped with Andor iDus Si and InGaAs CCD array detectors. Photoexcitation was achieved with a 405 nm diode laser (ca. 2 mm spot size, 1.95 mW).

Time-correlated single-photon counting (TCSPC) was performed by exciting samples with a PicoQuant picosecond diode laser (λ_{exc} = 407 nm, 10 MHz repetition rate, 278 µW). An Edinburgh Instruments Life Spec system equipped with a Hamamatsu photomultiplier tube was used for photoluminescence detection, with an instrument response time of less than 150 ps. To minimise pump scatter in the photoluminescence path, a 435 nm long-pass filter was placed before the monochromator.

B. COF syntheses

Reagents and solvents were obtained in high-purity grades from commercial suppliers and were, unless shipped under argon, degassed and saturated with argon prior to use. The COF building blocks were synthesized as detailed in Section C. 1,1,2,2-tetrakis(4-aminophenyl)ethene (4PE(NH_2)$_4$) was synthesized as reported previously.[2] Thieno[3,2-*b*]thiophene-2,5-dicarbaldehyde (TT(CHO)$_2$) was obtained from Merck and purified by recrystallisation from hot DMF. Please refer to page S1 for a list of abbreviations for the COF building blocks and solvents.

COF bulk powder syntheses were performed under N_2 atmosphere in PTFE-sealed glass reaction tubes (6 mL volume).

COF thin films were synthesized in 100 mL autoclaves equipped with a 28 mm diameter glass liner. Fused silica, *c*-cut sapphire and ITO-coated glass substrates were cleaned in detergent solution (Hellmanex III), water, acetone, and isopropanol, and activated with an O_2-plasma for 5 min directly before use. The substrates were placed horizontally in PTFE sample holders with the activated surface face-down.

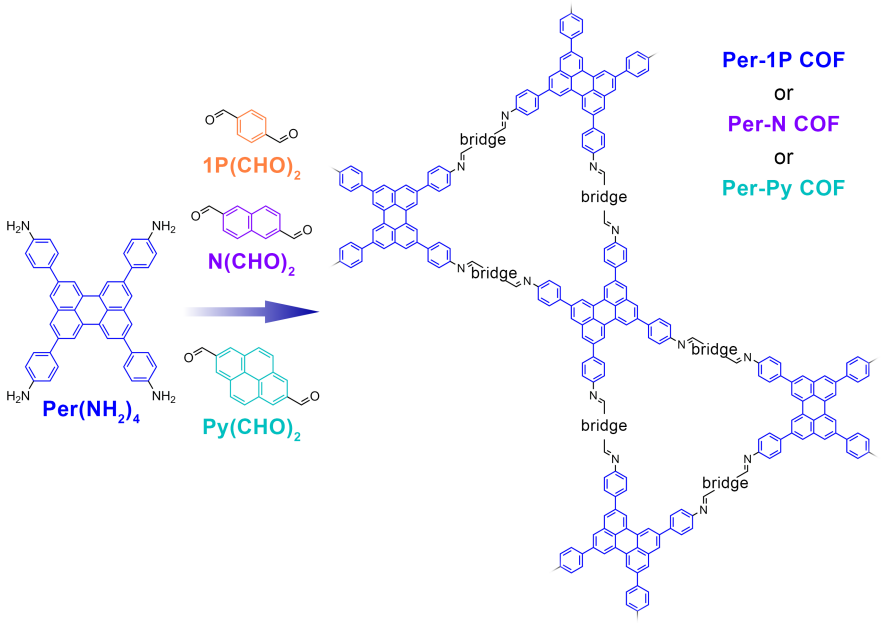

Figure S1-1. Construction of the new perylene COFs. The co-condensation of the tetradentate Per(NH_2)$_4$ with the linear phenylene, naphthalene or pyrene dicarboxaldehydes yields the star-shaped dual-pore Per-1P, Per-N and Per-Py COFs, respectively.

Per-1P COF. Per(NH_2)$_4$ (12.3 mg, 20 µmol, 1.0 eq.) and terephthalaldehyde (5.4 mg, 40 µmol, 2.0 eq.) were filled into a reaction tube, followed by the addition of mesitylene (333 µL), 1,4-dioxane (167 µL), and 6 M acetic acid (100 µL). The tube was sealed and heated at 120 °C for 6 d. After cooling to room temperature, the precipitate was collected by filtration, washed with MeCN and dried in argon to yield the COF as a light orange powder.

Per-1P COF films. An autoclave was charged with terephthalaldehyde (2.7 mg, 20 µmol, 2.0 eq.) and mesitylene (2667 µL). Next, a suspension of Per(NH_2)$_4$ (6.2 mg, 10 µmol, 1.0 eq.) in benzyl alcohol (1333 µL) was added. A fused silica substrate was inserted, followed by the addition of 6 M acetic acid (400 µL). The autoclave was sealed and heated at 120 °C for 2 d. After cooling to room temperature, the COF film was immersed in dry MeCN for 5 min and dried with a stream of nitrogen.

Per-N COF. Per(NH_2)$_4$ (12.3 mg, 20 µmol, 1.0 eq.) and N(CHO)$_2$ (7.4 mg, 40 µmol, 2.0 eq.) were filled into a reaction tube, followed by the addition of mesitylene (333 µL), benzyl alcohol (167 µL), and 6 M acetic acid (100 µL). The tube was sealed and heated at 120 °C for 6 d. After cooling to room temperature, the precipitate was collected by filtration, washed with MeCN and dried in argon to yield the COF as a bright orange powder.

Per-N COF films. An autoclave was charged with N(CHO)$_2$ (3.7 mg, 20 µmol, 2.0 eq.) and mesitylene (2667 µL). Next, a suspension of Per(NH_2)$_4$ (6.2 mg, 10 µmol, 1.0 eq.) in benzyl alcohol (1333 µL) was added. A fused silica substrate was inserted, followed by the addition of 6 M acetic acid (400 µL). The autoclave was sealed and heated at 120 °C for 2 d. After cooling to room temperature, the COF film was immersed in dry MeCN for 5 min and dried with a stream of nitrogen.

Per-Py COF. Per$(NH_2)_4$ (12.3 mg, 20 µmol, 1.0 eq.) and Py$(CHO)_2$ (10.3 mg, 40 µmol, 2.0 eq.) were filled into a reaction tube, followed by the addition of mesitylene (333 µL), 1,4-dioxane (167 µL), and 6 M acetic acid (100 µL). The tube was sealed and heated at 120 °C for 6 d. After cooling to room temperature, the precipitate was collected by filtration, washed with MeCN and dried in argon to yield the COF as a bright yellow powder.

Per-Py COF films. An autoclave was charged with Py$(CHO)_2$ (5.2 mg, 20 µmol, 2.0 eq.) and mesitylene (2667 µL). Next, a suspension of Per$(NH_2)_4$ (6.2 mg, 10 µmol, 1.0 eq.) in benzyl alcohol (1333 µL) was added. A fused silica substrate was inserted, followed by the addition of 6 M acetic acid (400 µL). The autoclave was sealed and heated at 120 °C for 2 d. After cooling to room temperature, the COF film was immersed in dry MeCN for 5 min and dried with a stream of nitrogen.

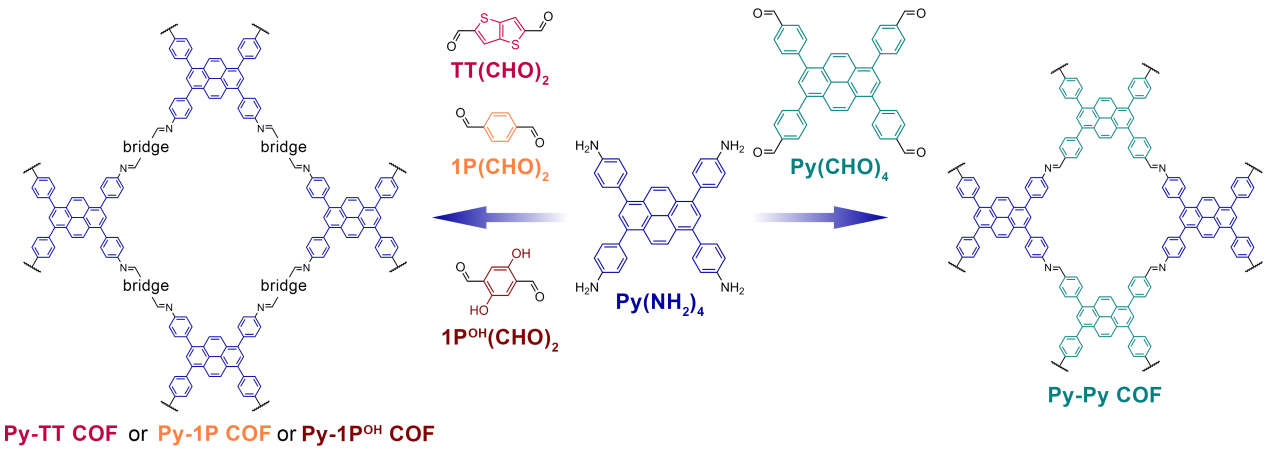

Figure S1-2. Synthesis of the pyrene COFs. The combination of the tetraaniline with linear dicarboxaldehydes yields pseudo-square COFs with two imines per bridge unit,[3-5] whereas the co-condensation with the pyrene tetraaldehyde produces a framework of similar overall topology, but with only one imine between adjacent pyrenes.[4]

Py-TT COF films. An autoclave was charged with Py$(NH_2)_4$(dioxane)$_{1.5}$ (7.0 mg, 10 µmol, 1.0 eq.), TT$(CHO)_2$ (3.9 mg, 20 µmol, 2.0 eq.), mesitylene (1333 µL) and benzyl alcohol (667 µL). A fused silica substrate was inserted, followed by the addition of 6 M acetic acid (200 µL). The autoclave was sealed and heated at 120 °C for 3 d. After cooling to room temperature, the COF film was rinsed with dry MeCN and dried with compressed air.

The bulk synthesis of this COF has been reported previously.[4]

Py-1P COF films. An autoclave was charged with Py$(NH_2)_4$(dioxane)$_{1.5}$ (7.0 mg, 10 µmol, 1.0 eq.), terephthalaldehyde (2.7 mg, 20 µmol, 2.0 eq.), mesitylene (1333 µL) and benzyl alcohol (667 µL). An ITO substrate was inserted, followed by the addition of 6 M acetic acid (200 µL). The autoclave was sealed and heated at 120 °C for 3 d. After cooling to room temperature, the COF film was rinsed with dry MeCN and dried with compressed air.

The bulk synthesis of this COF has been reported previously.[3-4]

Py-1P^{OH} COF.[5] Py$(NH_2)_4$(dioxane)$_{0.85}$ (12.8 mg, 20 µmol, 1.0 eq.) and 1P^{OH}$(CHO)_2$ (6.6 mg, 40 µmol, 2.0 eq.) were filled into a reaction tube, followed by the addition of mesitylene (667 µL), 1,4-dioxane (333 µL), and 6 M acetic acid (100 µL). The tube was sealed and heated at 120 °C for 5 d. After cooling to room temperature, the precipitate was collected by filtration, washed with MeCN and dried in argon to yield the COF as an orange powder.

Py-1P^{OH} COF films. An autoclave was charged with Py$(NH_2)_4$(dioxane)$_{1.5}$ (7.0 mg, 10 µmol, 1.0 eq.), 1P^{OH}$(CHO)_2$ (3.3 mg, 20 µmol, 2.0 eq.), mesitylene (667 µL) and benzyl alcohol (1333 µL). A substrate (fused silica or ITO) was inserted, followed by the addition of 6 M acetic acid (200 µL). The autoclave was sealed and heated at 120 °C for 3 d. After cooling to room temperature, the COF film was rinsed with dry MeCN and dried with compressed air.

Py-Py COF films. An autoclave was charged with $Py(NH_2)_4(dioxane)_{0.85}$ (12.8 mg, 20 µmol, 1.0 eq.), $Py(CHO)_4$ (12.4 mg, 20 µmol, 1.0 eq.), mesitylene (2667 µL) and benzyl alcohol (1333 µL). A substrate (fused silica or ITO) was inserted, followed by the addition of 6 M acetic acid (400 µL). The autoclave was sealed and heated at 120 °C for 3 d. After cooling to room temperature, the COF film was rinsed with dry MeCN and dried with a stream of nitrogen.

The bulk synthesis of this COF has been reported previously.[4]

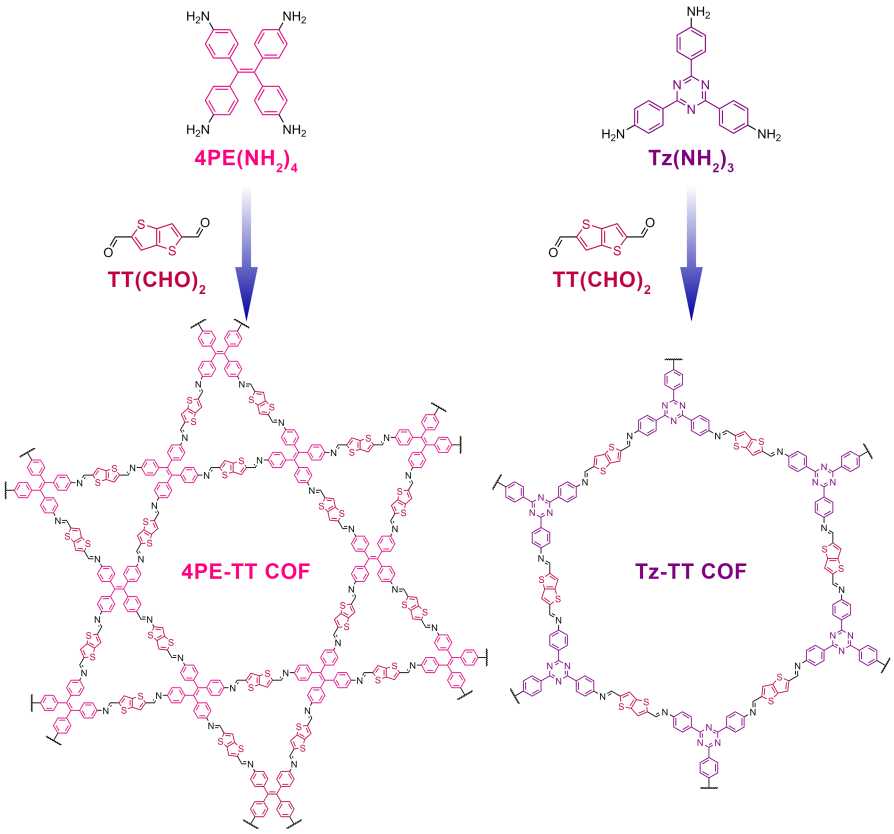

Figure S1-3. Construction of the hexagonal COFs. The propeller-shaped tetraphenylethene building block gives rise to the 4PE-TT COF with a star-shaped topology,[2] while the trigonal tetraphenyltriazine yields the new Tz-TT COF.

4PE-TT COF films. An autoclave was charged with $4PE(NH_2)_4$ (5.9 mg, 15 µmol, 1.0 eq.), $TT(CHO)_2$ (5.9 mg, 30 µmol, 2.0 eq.), mesitylene (200 µL) and benzyl alcohol (1800 µL). A substrate (fused silica or sapphire) was inserted, followed by the addition of 6 M acetic acid (200 µL). The autoclave was sealed and heated at 120 °C for 3 d. After cooling to room temperature, the COF film was rinsed with dry MeCN and dried with compressed air.

The bulk synthesis of this COF has been reported previously.[2]

Tz-TT COF. $Tz(HN_2)_3$ (10.6 mg, 30 µmol, 1.0 eq.) and $TT(CHO)_2$ (8.8 mg, 45 µmol, 1.5 eq.) were filled into a reaction tube, followed by the addition of mesitylene (667 µL), benzyl alcohol (333 µL), and 6 M acetic acid (40 µL). The tube was sealed and heated at 120 °C for 3 d. The supernatant was removed and the precipitate was extracted with supercritical CO_2 (40 °C, 90 bar, 2 h) to yield the COF as an orange powder.

Tz-TT COF films. An autoclave was charged with $Tz(HN_2)_3$ (3.5 mg, 10 µmol, 1.0 eq.), $TT(CHO)_2$ (2.9 mg, 15 µmol, 1.5 eq.), mesitylene (1333 µL) and benzyl alcohol (667 µL). A fused silica substrate was inserted, followed by the addition of 6 M acetic acid (80 µL). The autoclave was sealed and heated at 120 °C for 3 d. After cooling to room temperature, the COF film was rinsed with dry MeCN and dried with compressed air.

C. Building block syntheses

All reactions were performed in oven-dried glassware under argon atmosphere using standard Schlenk and glovebox techniques. Reagents and solvents were obtained in high-purity grades from commercial suppliers and were, unless shipped under argon, degassed and saturated with argon prior to use.

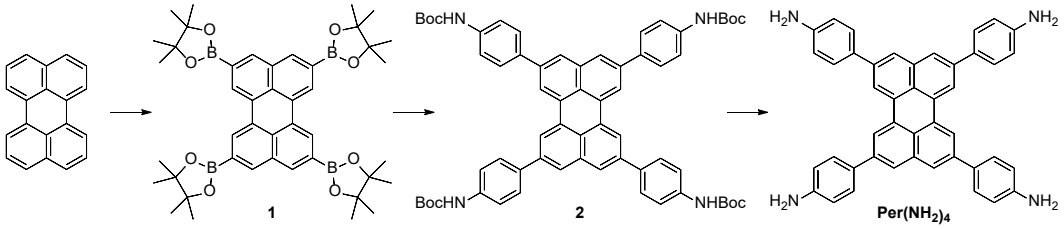

Figure S2. Synthesis of the new tetrakis(4-aminophenyl)perylene building block.

2,5,8,11-tetrakis(4,4,5,5-tetramethyl-1,3,2-dioxaborolan-2-yl)perylene (1)[6]

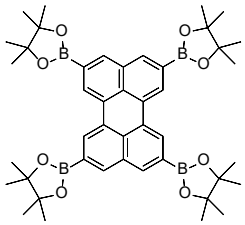

A reaction mixture containing perylene (2019 mg, 8.00 mmol, 1.0 eq.), $[Ir(OMe)(1,5\text{-cod})]_2$ (265 mg, 0.40 mmol, 5 mol%), 4,4'-di-*tert*-butyl-2,2'-bipyridyl (215 mg, 0.80 mmol, 10 mol%), and bis(pinacolato)diboron (9751 mg, 38.4 mmol, 4.8 eq.) in 64 mL anhydrous cyclohexane was stirred under argon at 80 °C for 40 h. After cooling to room temperature, the yellow precipitate was collected by filtration, washed with cyclohexane and acetone to yield the title compound as a bright yellow powder (5732 mg, 7.580 mmol, 95%). The material was used directly in the next step without further purification.

^{1}H NMR (400 MHz, $CDCl_3$): 8.63 (s, 4H), 8.25 (s, 4H), 1.43 (s, 48H).

^{13}C NMR (100 MHz, $CDCl_3$): 137.1, 133.4, 132.1, 130.5, 126.6 (br.), 126.2, 84.2, 25.1.

2,5,8,11-tetrakis(4-Boc-aminophenyl)perylene (2)

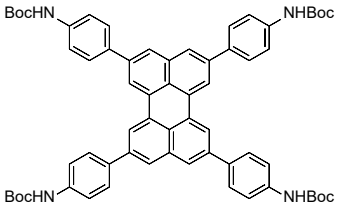

A reaction mixture containing compound **1** (1512 mg, 2.00 mmol, 1.0 eq.), *N*-Boc-4-bromoaniline (8708 mg, 32.0 mmol, 16 eq.), K_2CO_3 (2211 mg, 16.0 mmol, 8.0 eq.), $Pd_2(dba)_3{\cdot}CHCl_3$ (414 mg, 0.40 mmol, 20 mol%), and Sphos (328 mg, 0.80 mmol, 40 mol%) in 64 mL *o*-xylene and 16 mL H_2O was stirred under a static argon atmosphere at 100 °C for 40 h. After cooling to room temperature, 20 mL MeOH was added to form a homogeneous suspension. The precipitate was collected by filtration and washed with H_2O and MeOH until the washings were clear. The greenish solid was dissolved in a 6:4 DCM/EtOAc mixture and passed through a short plug of silica gel. The solution was concentrated to ca. 20 mL under reduced pressure, causing the product to precipitate. The precipitate was collected by filtration and washed successively with 10 mL MeOH and 10 mL DCM. For further purification, the product was dispersed in 600 mL EtOAc and sonicated for 30 min. The suspension was concentrated to ca. 20 mL under reduced pressure. The solids were collected by filtration, washed successively with 10 mL EtOAc and 10 mL DCM, and dried under high vacuum to yield the title compound as a greenish-yellow powder (1298 mg, 1.28 mmol, 64%).

^{1}H NMR (400 MHz, DMSO-d_6): 9.52 (s, 4H), 8.73 (s, 4H), 8.14 (s, 4H), 7.92 (d, J = 8.6 Hz, 8H), 7.66 (d, J = 8.3 Hz, 8H), 1.52 (s, 36H).

Due to the low solubility of this compound, no ^{13}C NMR spectra were recorded.

2,5,8,11-tetrakis(4-aminophenyl)perylene, Per(NH_2)$_4$

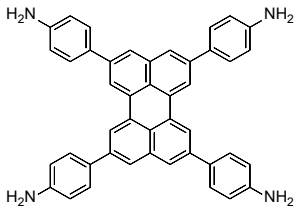

To a suspension of compound **2** (829 mg, 0.82 mmol, 1.0 eq.) in 30 mL anhydrous DCM was added 10 mL TFA. The resulting dark yellow solution was stirred for 2 h at room temperature. The reaction mixture was neutralised by slow addition of a saturated $NaHCO_3$ solution in argon-saturated H_2O, causing the product to precipitate as a dark orange solid. The solids were collected by filtration, washed with 500 mL argon-saturated H_2O and dried under high vacuum to yield the title compound as a bright orange powder (487 mg, 0.79 mmol, 97%).

^{1}H NMR (400 MHz, DMSO-d_6): 8.55 (s, 4H), 7.95 (s, 4H), 7.69 (d, J = 8.4 Hz, 8H), 6.76 (d, J = 8.6 Hz, 8H), 5.32 (s, 8H).

^{13}C NMR (100 MHz, DMSO-d_6): 148.7, 139.1, 135.6, 130.7, 127.8, 127.1, 125.2, 123.7, 118.4, 114.2.

naphthalene-2,6-dicarbaldehyde

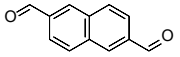

2,6-Dibromonaphthalene (1000 mg, 3.50 mmol, 1.0 eq.) was dissolved in 35 mL anhydrous THF and cooled to -84 °C. *n*-BuLi (2.5 M in hexanes, 14 mmol, 4.0 eq.) was added dropwise and the solution was stirred for 45 min at -84 °C and 1.5 h at 0 °C. Subsequently, anhydrous DMF (5.4 mL, 70 mmol, 20 eq.) was added dropwise and the resulting suspension was allowed to warm to room temperature over the course of 1h. The reaction was quenched with saturated aqueous NH_4Cl and extracted with DCM. The organic phase was dried over $MgSO_4$ and concentrated under reduced pressure. Purification via flash column chromatography (silica gel, DCM + 2% EtOAc), followed by crystallisation from $CHCl_3$ (20 mL) and cyclohexane (40 mL) yielded the title compound as colourless needles (256 mg, 1.39 mmol, 40%).

^{1}H NMR (400 MHz, $CDCl_3$): 10.22 (s, 2H), 8.50 – 8.30 (m, 2H), 8.13 (d, J = 8.4 Hz, 2H), 8.06 (dd, J = 8.4, 1.4 Hz, 2H).

^{13}C NMR (100 MHz, $CDCl_3$): 191.9, 136.3, 135.9, 133.8, 130.8, 124.3.

pyrene-2,7-dicarbaldehyde

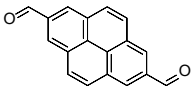

2,7-dibromopyrene (1000 mg, 2.78 mmol, 1.0 eq.) was dissolved in 111 mL anhydrous THF and cooled to -84 °C. *n*-BuLi (2.5M in hexanes, 11.2 mmol, 4.0 eq.) was added dropwise and the reaction mixture was stirred for 10 min at -84 °C and 50 min at 0 °C. Anhydrous DMF (4.3 mL, 55.6 mmol, 20 eq.) was added dropwise at 0 °C and the resulting suspension was allowed to warm to room temperature overnight. The reaction was quenched with H_2O, extracted with $CHCl_3$, dried over $MgSO_4$, and passed through a short plug of silica gel using $CHCl_3$ as the eluent. Crystallisation from $CHCl_3$/heptane yielded the title compound as light green needles (123 mg, 0.48 mmol, 17%).

^{1}H NMR (400 MHz, $CDCl_3$): 10.48 (s, 2H), 8.72 (s, 4H), 8.27 (s, 4H).

1,3,6,8-tetrakis(4-aminophenyl)pyrene, Py(NH_2)$_4$[3, 7]

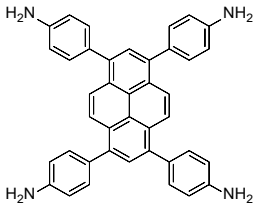

A reaction mixture containing 1,3,6,8-tetrabromopyrene (1482 mg, 2.86 mmol, 1.0 eq.), 4-aminophenylboronic acid pinacol ester (3010 mg, 13.7 mmol, 4.8 eq.), K_2CO_3 (2175 mg, 15.7 mmol, 5.5 eq.), and $Pd(PPh_3)_4$ (330 mg, 0.29 mmol, 10 mol%) in 32 mL 1,4-dioxane and 8 mL H_2O was refluxed at 115 °C for 3 d under a static argon atmosphere (regulated to 0.1 bar overpressure vs. air). After cooling to room temperature, 60 mL H_2O was added under argon. After 2 h the precipitate was collected by filtration and washed with H_2O and MeOH until the washings were clear. The resulting yellow-green powder was dried under high vacuum and re-dissolved in 75 mL 1,4-dioxane at 105 °C. This solution was cooled to room temperature, mixed with 20 mL acetone, filtered through a 0.45 µm GXF/GHP membrane filter (Acrodisc), and dried under reduced pressure. The product

was crystallized from 1,4-dioxane (105 °C to room temperature) and dried under high vacuum, yielding the title compound, co-crystallized with approximately 0.85 dioxane molecules per formula unit, as a bright yellow powder (1810 mg, 2.82 mmol, 98%).

^{1}H NMR (400 MHz, DMSO-d_6): 8.13 (s, 4 H), 7.79 (s, 2 H), 7.35 (d, J = 8.4 Hz, 8 H), 6.78 (d, J = 8.4 Hz, 8 H), 5.31 (s, 8 H), 3.56 (s, 7 H, dioxane).

^{13}C NMR (100 MHz, DMSO-d_6): 148.2, 137.1, 131.0, 129.0, 127.6, 126.7, 126.1, 124.4, 113.9, 66.3 (dioxane).

1,3,6,8-tetrakis(4-formylphenyl)pyrene neopentyl acetal

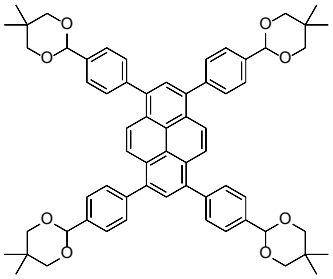

A reaction mixture containing 1,3,6,8-tetrabromopyrene (1139 mg, 2.20 mmol, 1.0 eq.), 4-formylphenylboronic acid neopentyl glycol ester neopentyl acetal (3212 mg, 10.6 mmol, 4.8 eq.), K_2CO_3 (1672 mg, 12.1 mmol, 5.5 eq.), and $Pd(PPh_3)_4$ (254 mg, 0.22 mmol, 10 mol%) in 16 mL 1,4-dioxane and 4 mL H_2O was refluxed at 115 °C for 3 d under argon. After cooling to room temperature, the reaction mixture was poured into water and extracted with $CHCl_3$. The organic phase was dried over $MgSO_4$, concentrated under reduced pressure and passed through a short plug of silica gel using DCM as eluent. Crystallisation from DCM/acetone yielded the product as a white powder (1602 mg, 1.66 mmol, 76%).

^{1}H NMR (400 MHz, $CDCl_3$): 8.12 (s, 4H), 7.92 (s, 2H), 7.72 – 7.64 (m, 16H), 5.53 (s, 4H), 3.84 (d, J = 11.2 Hz, 8H), 3.73 (d, J = 10.9 Hz, 8H), 1.36 (s, 12H), 0.84 (s, 12H).

^{13}C NMR (100 MHz, $CDCl_3$): 141.8, 137.7, 137.1, 130.8, 129.7, 128.3, 126.4, 126.0, 125.5, 101.8, 77.9, 30.5, 23.3, 22.1.

1,3,6,8-tetrakis(4-formylphenyl)pyrene, Py(CHO)$_4$

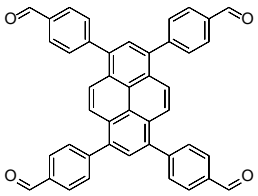

To a solution of 1,3,6,8-tetrakis(4-formylphenyl)pyrene neopentyl acetal (200 mg, 0.21 mmol, 1.0 eq.) dissolved in $CHCl_3$ (60 mL), trifluoroacetic acid (12 mL) and water (1.2 mL) were added dropwise and left to stir at room temperature for 16 h. The reaction was neutralised by dropwise addition into sat. $NaHCO_3$ (250 mL) and the $CHCl_3$ was removed under reduced pressure. The precipitate was collected by filtration and washed sequentially with water, EtOH, and EtOAc to yield the title compound as a yellow powder (110 mg, 0.18 mmol, 86%).

^{1}H NMR (400 MHz, $CDCl_3$): 10.16 (s, 4H), 8.18 (s, 4H), 8.09 (d, J = 8.2 Hz, 8H), 8.04 (s, 2H), 7.86 (d, J = 8.0 Hz, 8H).

2,5-dihydroxybenzene-1,4-dicarbaldehyde, 1P^{OH}(CHO)$_2$

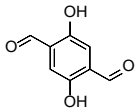

A solution of 2,5-dimethoxybenzene-1,4-dicarboxaldehyde (388 mg, 2.00 mmol, 1.0 eq.) in 20 mL anhydrous DCM was cooled to 0 °C in an ice bath. BBr_3 (771 µL, 8.00 mmol, 4.0 eq.) was added dropwise and the solution was stirred for 30 min at 0 °C. The ice bath was removed and stirring continued for another 2 h at room temperature. All volatiles were removed under high vacuum (double LN_2-cooled cold traps required!) and the solid residue was quenched by addition of 40 mL of a H_2O/MeOH 4:1 mixture. The product was extracted with EtOAc (300 mL), washed with brine, dried over $MgSO_4$, and concentrated under reduced pressure. The product was purified by recrystallisation from EtOAc (45 mL, 95 °C to room temperature), collected by filtration, washed with DCM and heptane, and dried under high vacuum, yielding the title compound as orange microplatelets (314 mg, 1.89 mmol, 95%).

^{1}H NMR (400 MHz, DMSO-d_6): 10.31 (s, 2H), 10.28 (s, 2H), 7.22 (s, 2H).

^{13}C NMR (100 MHz, DMSO-d_6): 190.2, 152.8, 127.7, 115.1.

D. Supplementary COF structure analysis

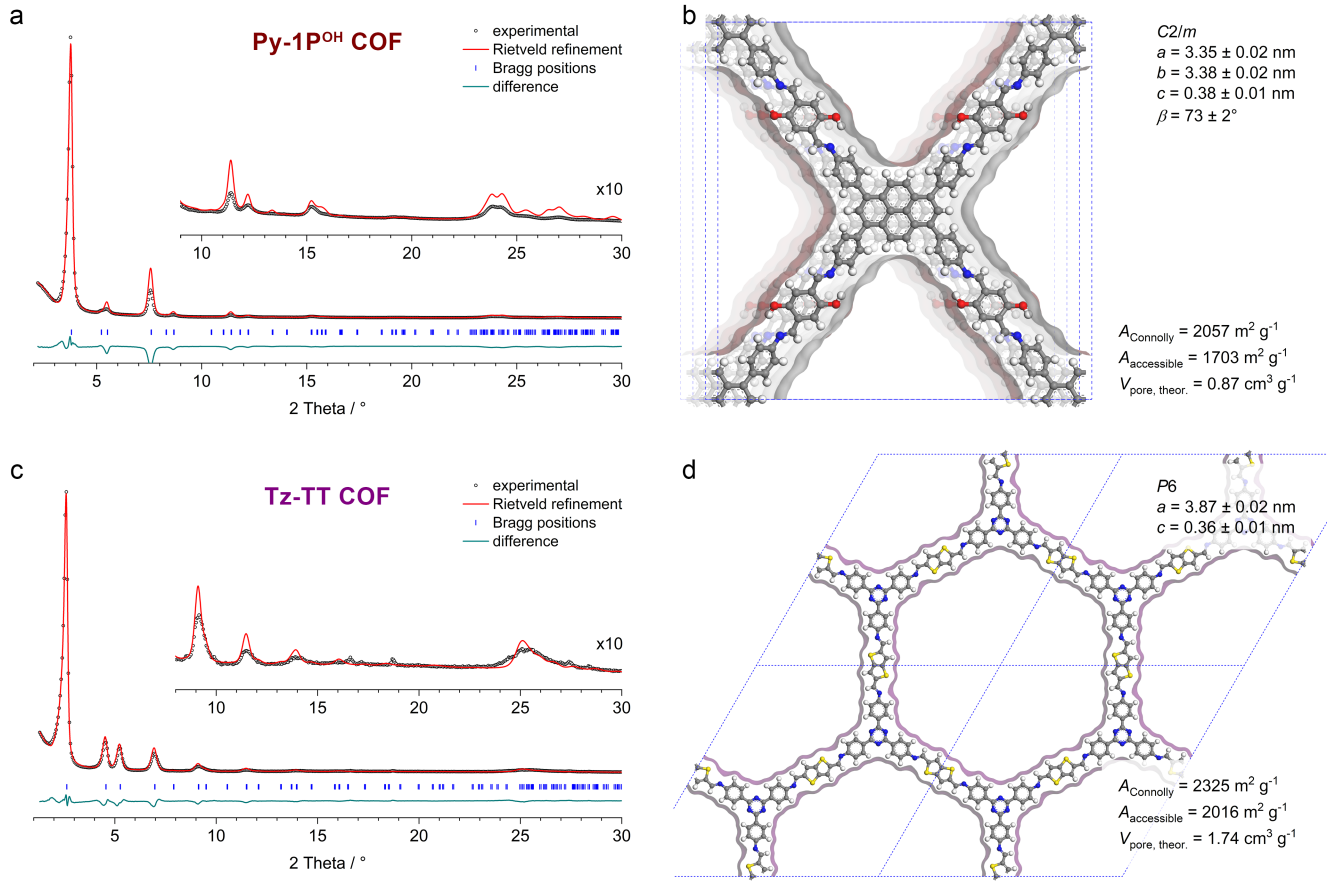

Figure S3-1. Structure analysis of the Py-1P^{OH} and Tz-TT COFs. (**a**) and (**c**), Experimental PXRD patterns (black dots) of the COF bulk materials. Rietveld refinements (red lines) using the structure models displayed in (**b**) and (**d**), respectively, provide very good fits to the experimental data with only small differences between the experimental and the refined patterns (green lines). Bragg positions are indicated by blue ticks. Insets, magnified view of the 2θ > 9° regions. (**b**) and (**d**), Structure models of the COFs. The viewing direction is normal to the crystallographic *a*-*b* plane.

The structure analysis of the Py-TT, Py-1P, Py-Py, and 4PE-TT COFs has been reported previously.[2-4]

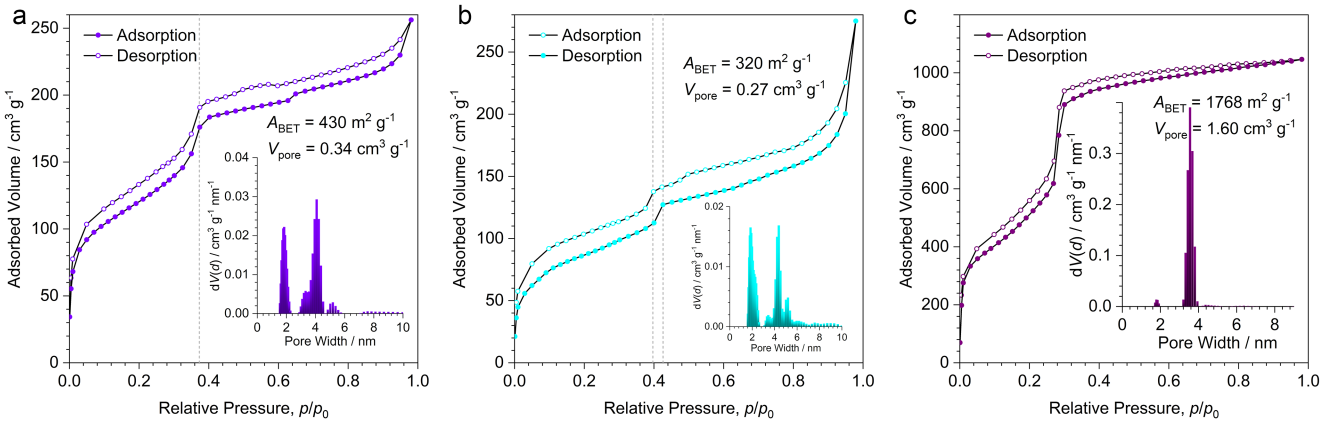

Figure S3-2. Nitrogen sorption isotherms of (**a**) the Per-N COF, (**b**) the Per-Py COF, and (**c**) the Tz-TT COF. The differences between the adsorption and the desorption branches are due to the inherent flexibility of the frameworks. The Per-N COF exhibits a reversible type IV(b) isotherm without hysteresis, which is typical for relatively small mesopores. The Per-Py COF, however, has a distinct hysteresis (grey dashed lines), indicating capillary condensation in its larger mesopores. Insets, pore size distributions calculated using a QSDFT equilibrium model. There are two maxima for the Per-N and Per-Py COFs which correspond to the smaller trigonal and the larger hexagonal pores, respectively. The porosity of the perylene COFs is reduced by oligomeric fragments that block some of the pores. These oligomers are due to the significantly higher reactivity of the perylene compared to the other aniline building blocks which results in a lower reversibility of the imine bonds.

E. GIWAXS analysis

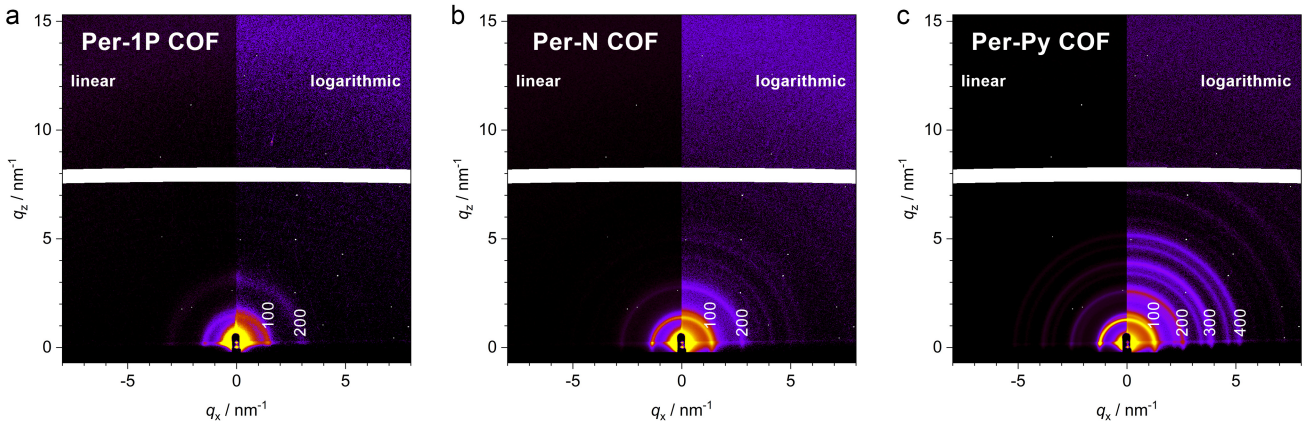

Figure S4-1. 2D GIWAXS patterns of the perylene COF films grown on fused silica substrates. (**a**) Per-1P COF. (**b**) Per-N COF. (**c**) Per-Py COF. The patterns are displayed using linear (left side) and logarithmic (right side) colour scaling. In contrast to the other COFs in this project, the individual crystallites in the polycrystalline perylene COF films are randomly oriented. We attribute this to the increased reactivity of the Per(NH_2)$_4$ building block over the other COF precursors, causing a significantly faster condensation of the perylene networks and reduced selectivity for specific crystal orientations. Our optical data show, however, that the pores in these COFs are fully accessible and that a specific orientation with respect to the substrate is not required for the application as acid sensors. The white area around q_z = 10 is due to the gap between the detector modules. The above GIWAXS patterns have been recorded after protonation with TFA vapour, followed by deprotonation with Et_3N solution and immersion in MeCN to remove the triethylammonium salt (Per-N COF: 4 protonation-deprotonation cycles).

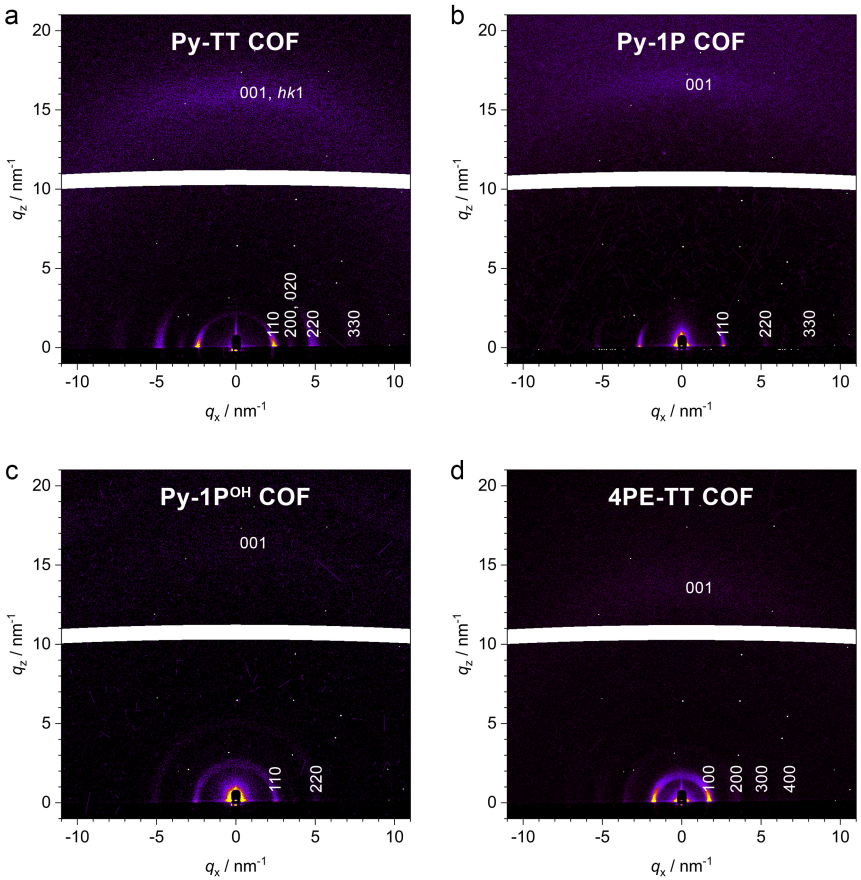

Figure S4-2. 2D GIWAXS patterns of the pyrene and tetraphenylethene COFs. (**a**) Py-TT COF on fused silica. (**b**) Py-1P COF grown on ITO-coated glass. (**c**) Py-1P^{OH} COF grown on fused silica. (**d**) 4PE-TT COF grown on *c*-cut sapphire. These COFs grow as polycrystalline films with planar disorder, i.e. the crystallographic *a*-*b* plane (the imine-linked layers) has a fixed orientation parallel to the substrate, but individual domains differ in their rotation about the substrate normal.

F. Perylene COFs UV-Vis and PL

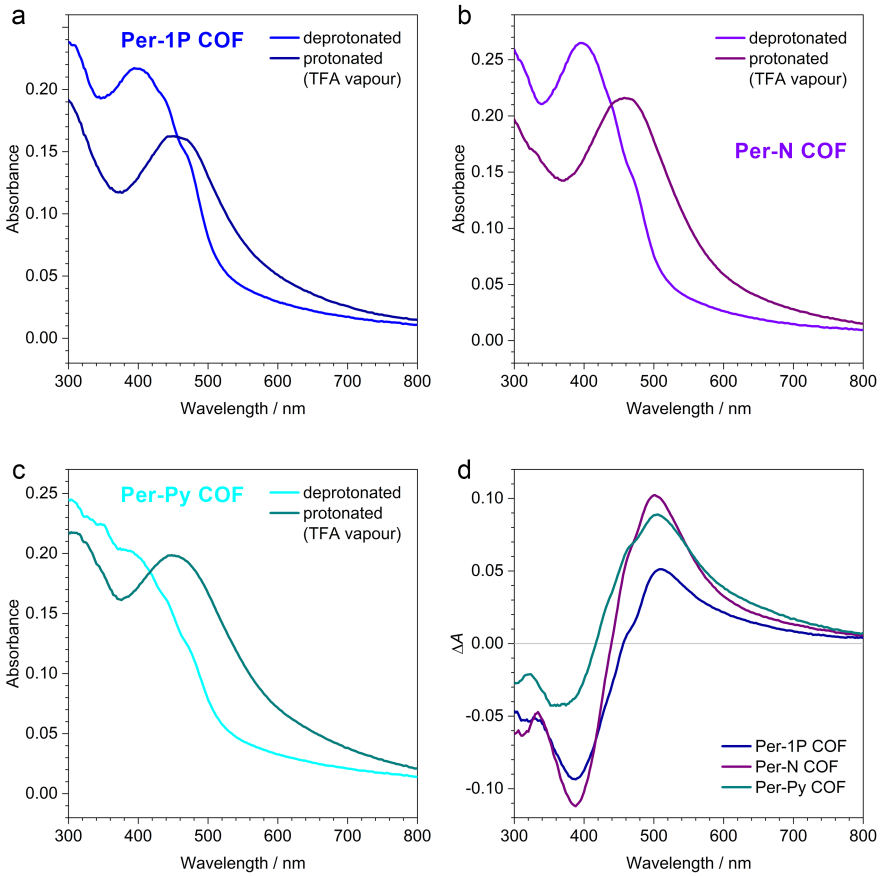

Figure S5-1. Protonation-dependent absorption changes of the perylene COFs. (**a**) Absorption spectra of a Per-1P COF film in air (blue) and after exposure to a saturated TFA atmosphere (dark blue). (**b**) Absorption spectra of a Per-N COF film in air (violet) and after exposure to a saturated TFA atmosphere (purple). (**c**) Absorption spectra of a Per-Py COF film in air (cyan) and after exposure to a saturated TFA atmosphere (dark green). (**d**) Comparison of the protonation-induced absorption changes. The spectra as well as the protonation-induced changes are quite similar across the perylene COF series, indicating that in these materials the optical properties are dominated by the perylene core.

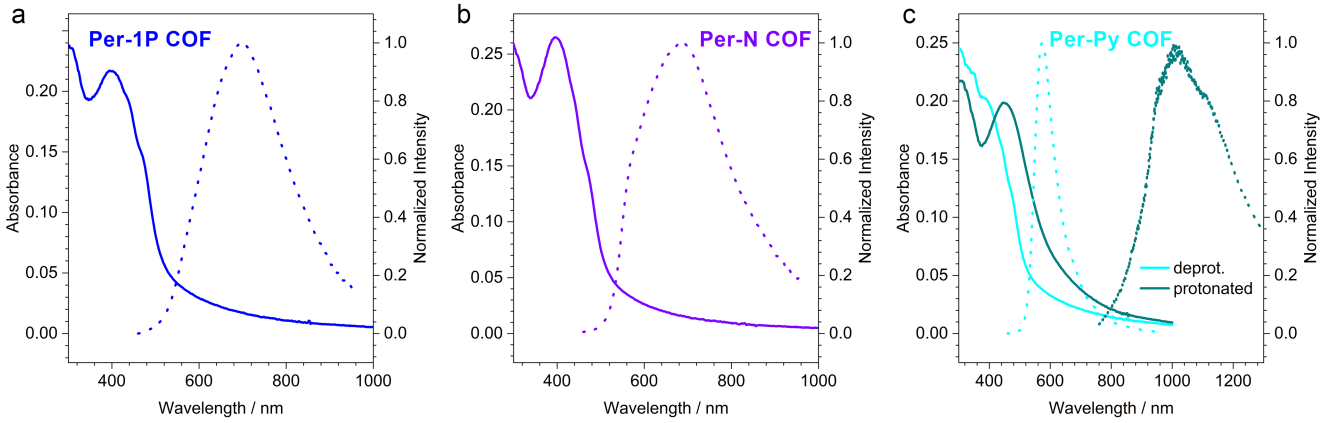

Figure S5-2. Absorption (solid lines) and PL spectra (dotted lines) of the perylene COFs. The deprotonated Per-1P (**a**) and Per-N COFs (**b**) exhibit a relatively weak and broad PL. The protonated COFs do not exhibit any measurable PL due to the increased core-to-imine charge-transfer character of the lowest-energy optical transitions. (**c**) The Per-Py COF has a much brighter and narrower emission than the other two COFs. In the protonated form, its emission is reduced in intensity by several orders of magnitude and shifted to around 1000 nm due to the increased charge-transfer character of the lowest-energy optical transitions.

G. PL lifetimes

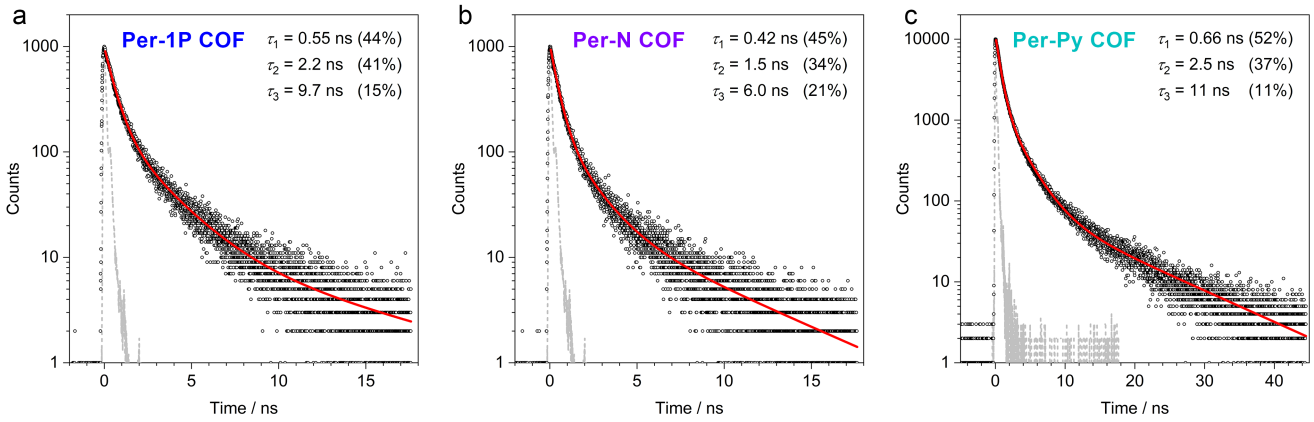

Figure S6. TCSPC decay traces of the three perylene-based COFs after photoexcitation at 407 nm. (**a**) Per-1P COF emission at 700 nm. (**b**) Per-N COF emission at 680 nm. (**c**) Per-Py COF emission at 570 nm. The COFs show three-exponential photoluminescence decays (red lines) with lifetimes ranging from around 0.5 ns for the shortest decay component to around 10 ns. The intensities of each decay component are stated in brackets. The instrument response function is shown in grey. The PL lifetimes of these COFs are at least 50% longer than those of similar pyrene- or porphyrin-based imine COFs.[3, 8-9] TCSPC data of the protonated COFs could not be recorded due to their extremely weak emission and wavelength limitations of common photon-counting detectors.

H. IR spectroscopy

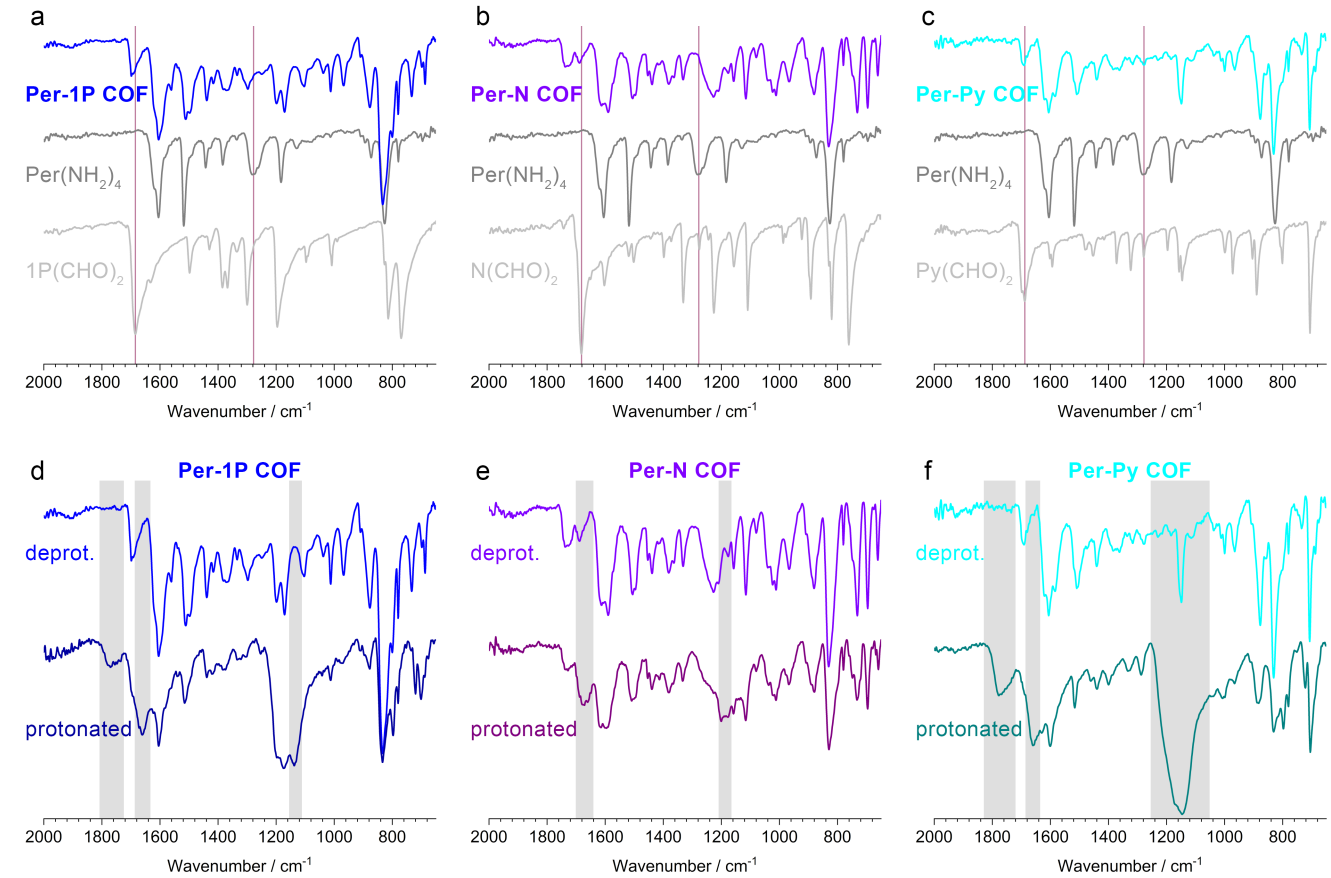

Figure S7. (**a**-**c**) Comparison of the perylene COFs (coloured lines) and their precursors (grey). The conversion of the aldehyde and amine functional groups is confirmed by the disappearance of the absorption bands at 1680 cm^{-1} and 1280 cm^{-1}, respectively (red vertical lines). (**d**-**f**) Comparison of the deprotonated and protonated perylene COF powders. The most apparent changes are highlighted in grey. The protonation leads to the appearance of the C=NH$^+$ stretching mode around 1650 cm^{-1}, accompanied by an attenuation of the imine C=N stretching mode around 1610 cm^{-1}.[10]

I. COF protonation – acid solution

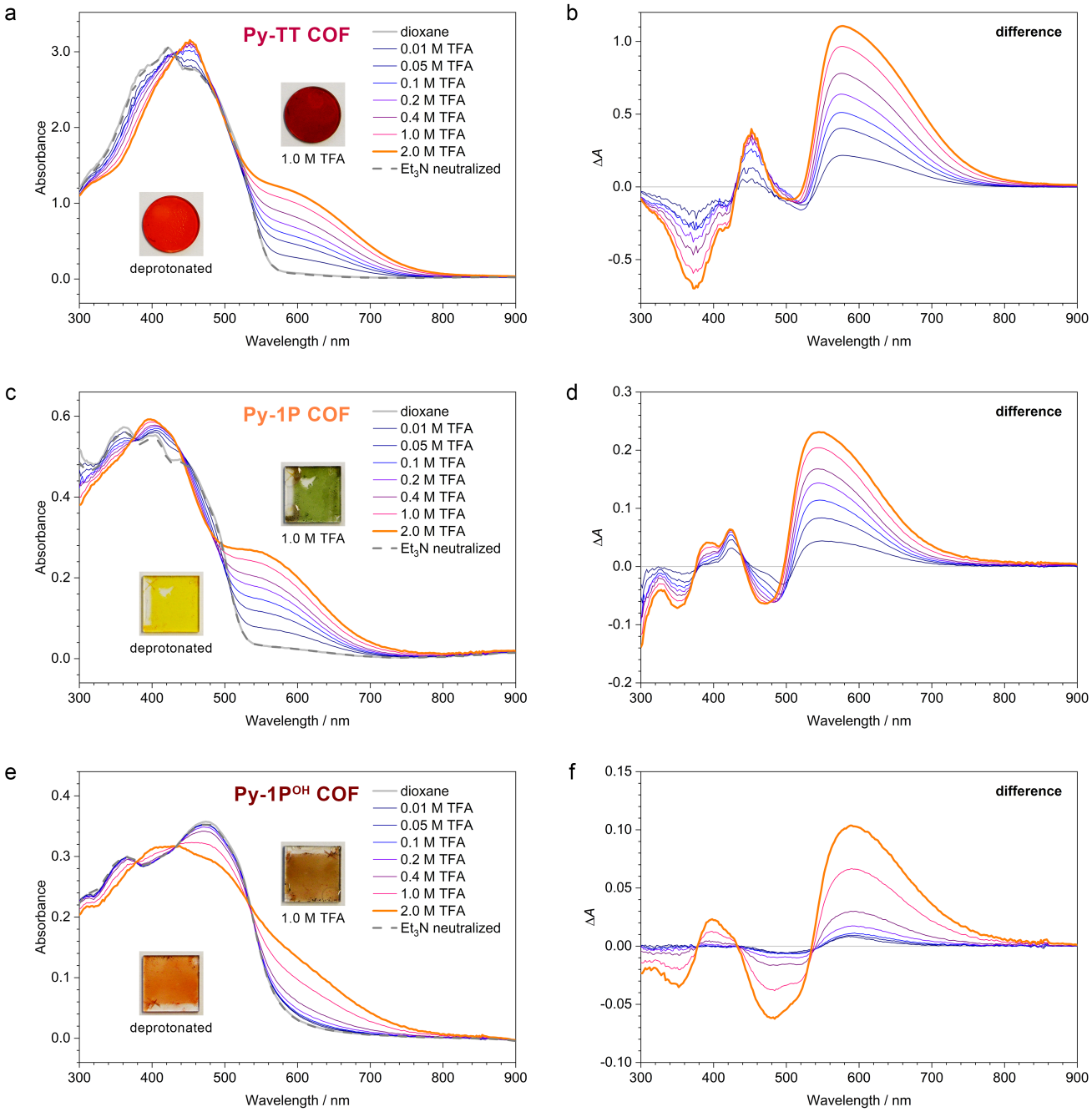

Figure S8-1. Protonation-induced spectral changes of the Py-TT COF (**a**, **b**), Py-1P COF (**c**, **d**) and Py-1P^{OH} COF (**e**, **f**). Left side, absorption spectra of the COF films in 1,4-dioxane (grey line) and in TFA solution of increasing concentration in 1,4-dioxane (blue to orange lines). The protonation can be fully reversed by immersing the COF films in a 0.5 M Et_3N solution in 1,4-dioxane (grey dashed line). The insets show the COF films in their deprotonated state and after mono-protonation with 1.0 M TFA solution. Right side, the absorption difference between the respective protonated spectra and the absorption of the non-protonated COFs. The shape of the spectra is independent of the acid concentration, indicating that the same protonated state is formed in this concentration range. The protonation of the Py-1P^{OH} COF is hindered by the competition between the protonated imine and the hydrogen bonds that stabilize the non-protonated state. Thus, this COF requires a considerably higher acid concentration to achieve any significant protonation.

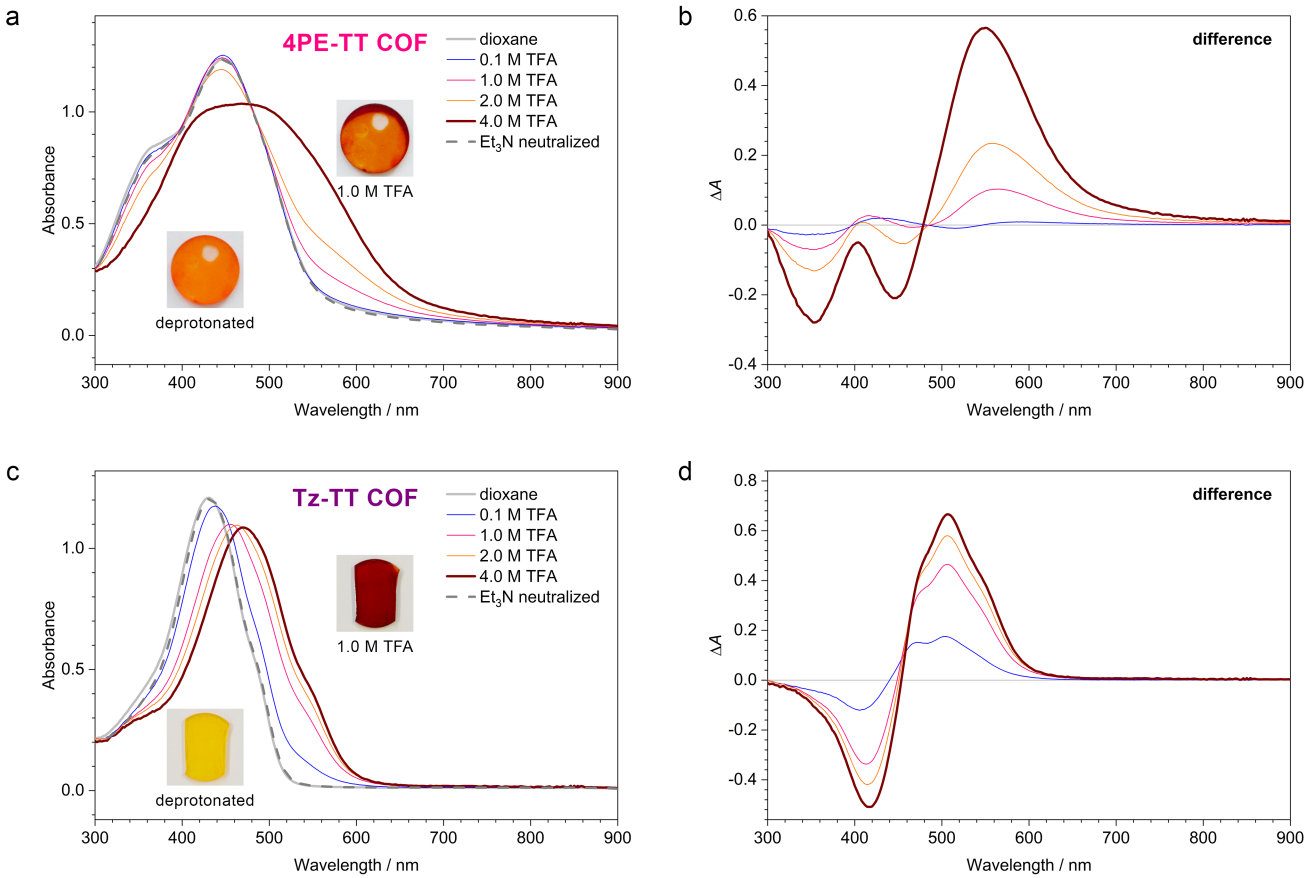

Figure S8-2. Protonation-induced spectral changes of the 4PE-TT COF (**a**, **b**) and the Tz-TT COF (**c**, **d**). Left side, absorption spectra of the COF films in 1,4-dioxane (grey line) and in TFA solution of increasing concentration in 1,4-dioxane (blue to orange lines). The protonation can be fully reversed by immersing the COF films in a 0.5 M Et_3N solution in 1,4-dioxane (grey dashed line). The insets show the COF films in their deprotonated state and after mono-protonation with 1.0 M TFA solution. Right side, the absorption difference between the protonated and the non-protonated COFs. The shape of the spectra is independent of the acid concentration, indicating that the same protonated state is formed in this concentration range.

J. Solvent-dependent protonation

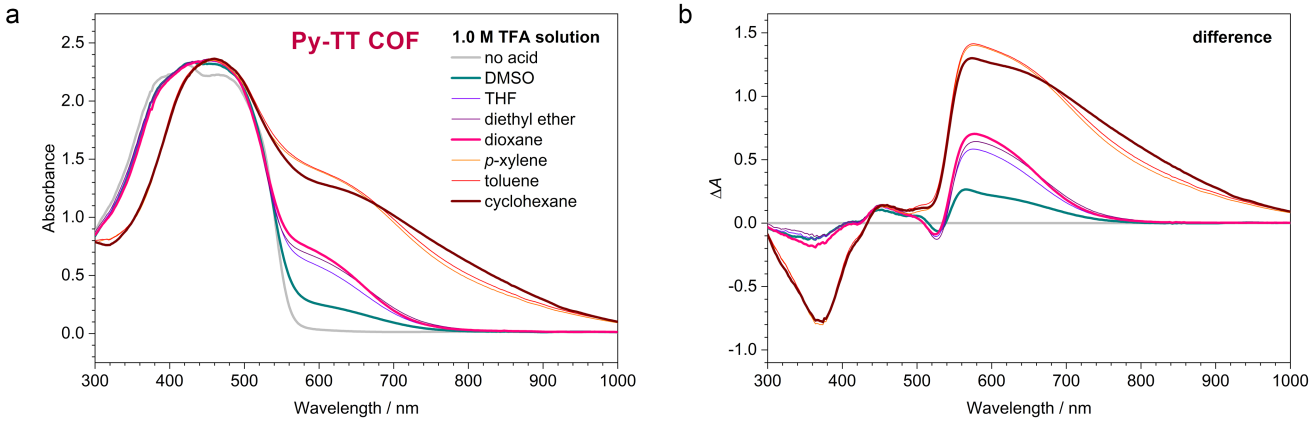

Figure S9. Protonation of the Py-TT COF using TFA solutions in different solvents. (**a**) The absorption spectra of the non-protonated COF film (grey) and after protonation in different solvents (coloured lines). (**b**) The corresponding absorption difference between the protonated and the non-protonated states. In DMSO, which is a good hydrogen bond acceptor, the protonation strength of the acid is reduced considerably and only a low concentration of the mono-protonated imine COF is generated. The ether solvents THF, diethyl ether and dioxane are less good hydrogen bond acceptors, but still have a levelling effect on the acid strength. Thus, although more imine bonds are protonated in total, only the mono-protonated species is formed. In the non-polar hydrocarbon solvents, which are very poor hydrogen bond acceptors, the acid strength of TFA is considerably higher and sufficient to generate the bis-protonated state (in coexistence with the mono-protonated form).

K. COF protonation – various acids

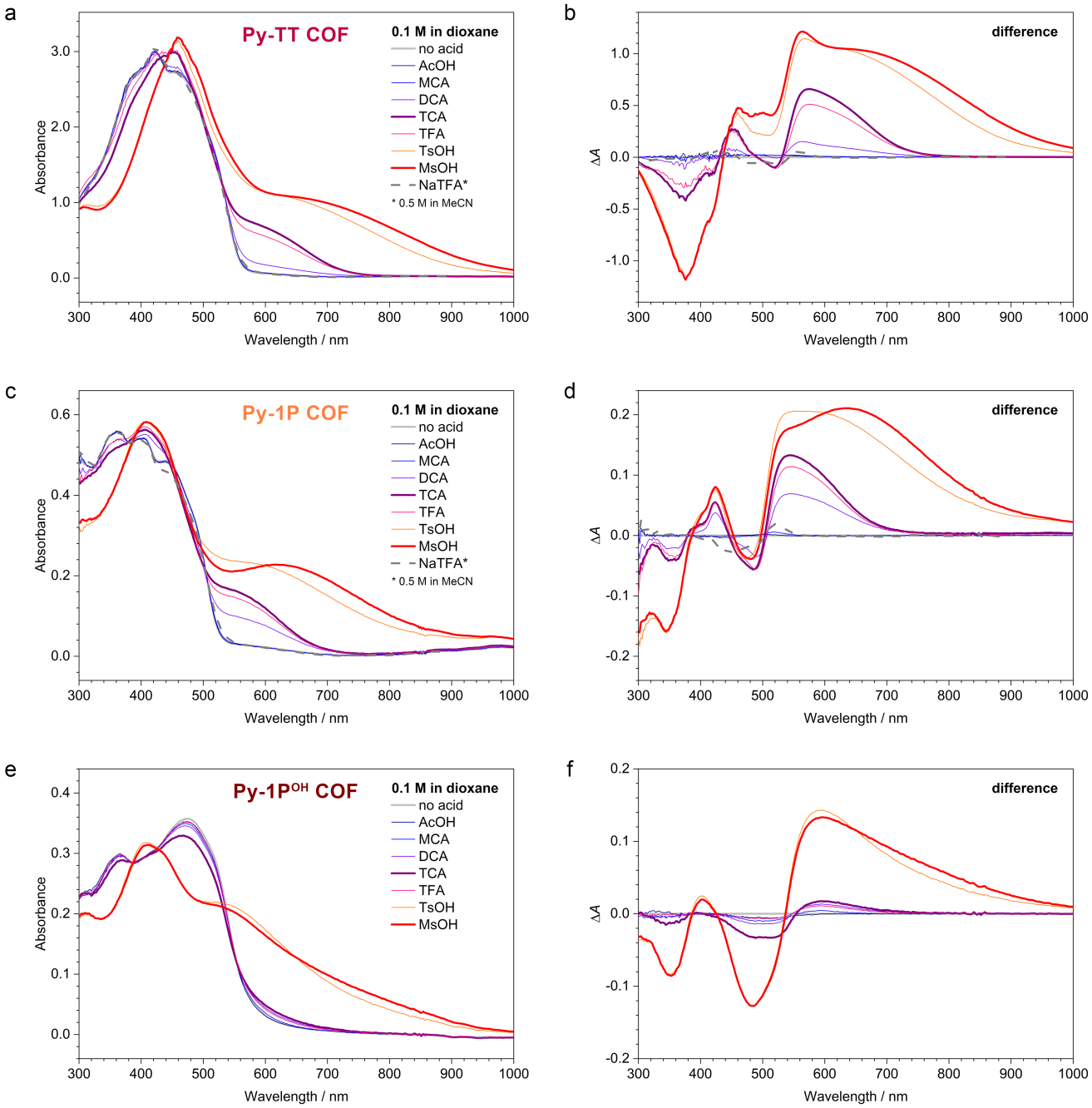

Figure S10. Protonation of the pyrene COF films in different acids. Left side, absorption spectra of the Py-TT COF (**a**), Py-1P COF (**c**) and Py-1P^{OH} COF (**e**) in 1,4-dioxane (grey line) and in a series of (halogenated) acetic acid and sulfonic acid solutions. Right side, the corresponding absorption differences between the protonated spectra and the absorption of the non-protonated COFs. While AcOH and MCA achieve hardly any protonation, immersing the COF films in DCA, TFA or TCA solutions causes an observable red-shifted absorption band. We attribute this absorption band to a mono-protonation of the phenylene-N=CH-bridge-HC=N-phenylene unit (see the discussion in the main article). The protonation of the Py-1P^{OH} COF is significantly hindered and thus the protonation bands have very low intensity (see the discussion in the article). For all three COFs, the sulfonic acids cause significantly stronger and spectrally different absorption bands. We attribute these differences to the formation of a bis-protonated state with further red-shifted absorption in addition to the mono-protonated state. Exposing the COF films to a solution of sodium trifluoroacetate instead has almost no effect on the absorption spectra, confirming that the contribution of solvatochromism to the spectral changes is negligible. Abbreviations: AcOH = acetic acid, MCA = chloroacetic acid, DCA = dichloroacetic acid, TCA = trichloroacetic acid, TFA = trifluoroacetic acid, TsOH = *p*-toluenesulfonic acid, MsOH = methanesulfonic acid.

L. COF stability

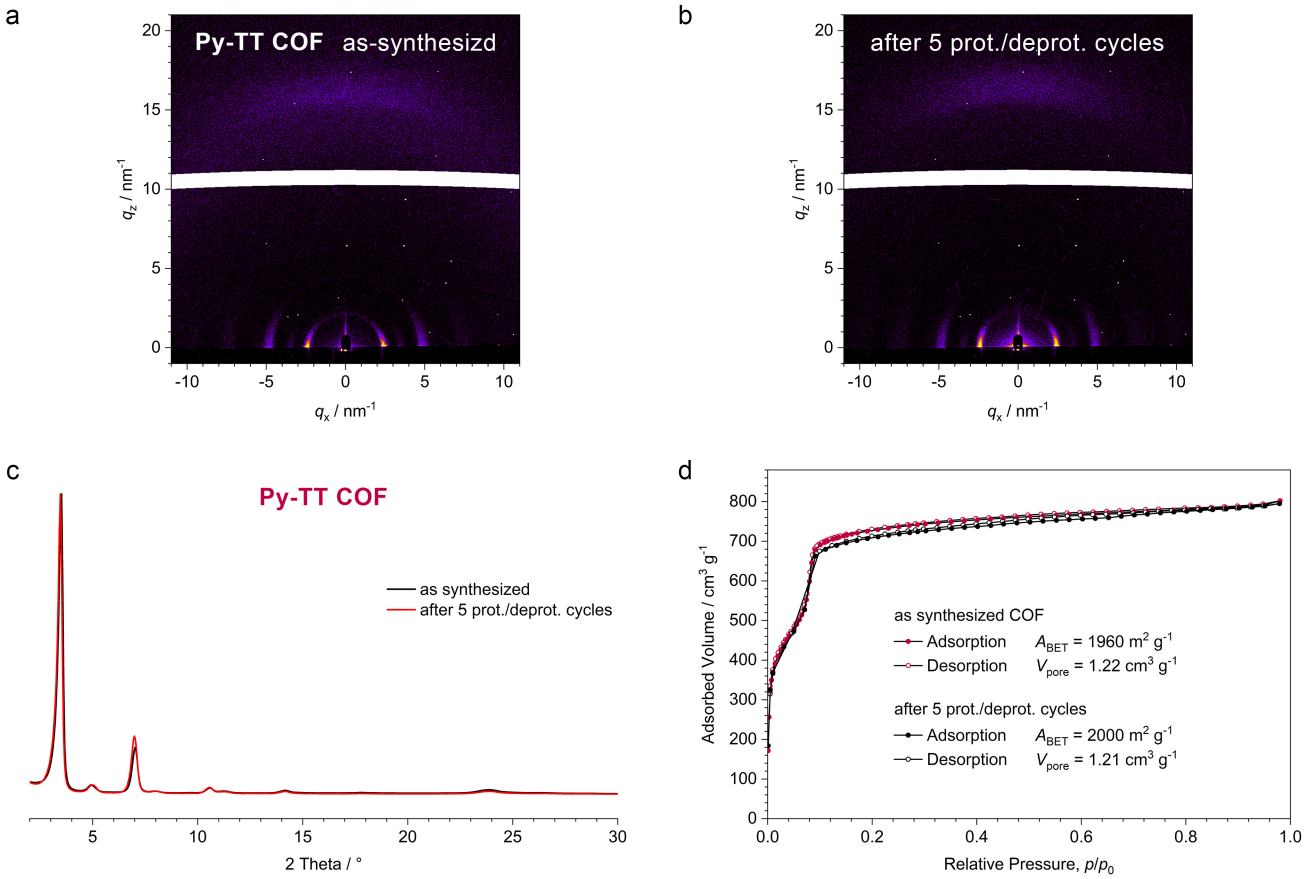

Figure S11-1. Stability of the COFs. (**a**) GIWAXS pattern of the as-synthesized 270 nm thick Py-TT COF film. (**b**) GIWAXS pattern of the film after five protonation/deprotonation cycles. The film does not show any signs of degradation. (**c**) PXRD patterns of Py-TT COF bulk powder before and after five protonation/deprotonation cycles with ca. 1M TFA and Et_3N solutions. (**d**) Nitrogen sorption isotherms of the as synthesized and the protonated/deprotonated Py-TT COF. The crystallinity and porosity are fully retained.

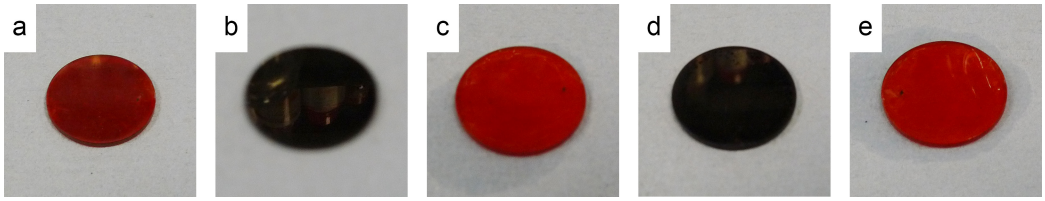

Figure S11-2. Repeated protonation and deprotonation of a 4PE-TT COF film using different bases. (**a**) The colour of the as-synthesized film is red-shifted by solvatochromism due to adsorbed water. (**b**) The COF film after protonation in TFA vapour. (**c**) After immersion in dilute NH_4OH in H_2O/MeOH 1:1. (**d**) Protonated again in TFA vapour. (**e**) After immersion in dilute KOH in MeOH. Exposure to the vapour/solution was ca. 2 s in each instance.

M. Py-Py COF mono-protonation

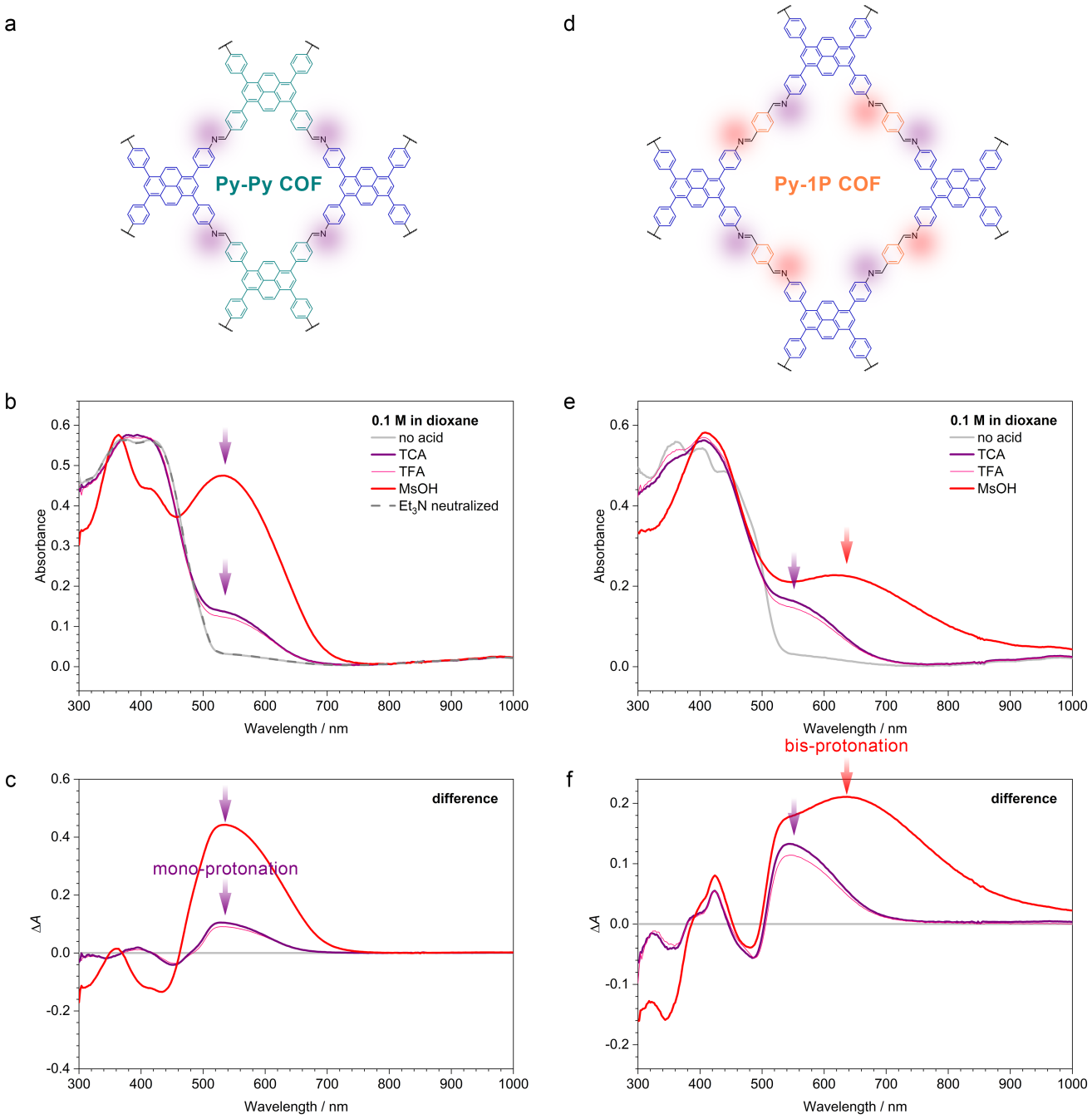

Figure S12. Protonation of the Py-Py and the Py-1P COFs. (**a**, **d**) Chemical structures of the COFs. The imine bonds are highlighted, indicating possible positions for the mono-protonation (purple) and successive bis-protonation (red). (**b**, **e**) Absorption spectra of the non-protonated framework and COF after protonation with different acids. Purple and red arrows indicate the main absorption signatures of the mono- and bis-protonated species, respectively. (**c**, **f**) Absorption difference between the protonated and the non-protonated COFs. While the combination of a tetradentate and a linear building block in the Py-1P COF generates the usual bridge units that contain two electronically correlated imines, the Py-Py COF is constructed from two complementary tetradentate building blocks and hence contains only one imine bond per bridge. Consequently, a bis-protonation is not possible and even the strongest sulfonic acids give rise to only the absorption band between 500 and 700 nm. Abbreviations: TCA = trichloroacetic acid, TFA = trifluoroacetic acid, MsOH = methanesulfonic acid.

N. Acid vapour sensing

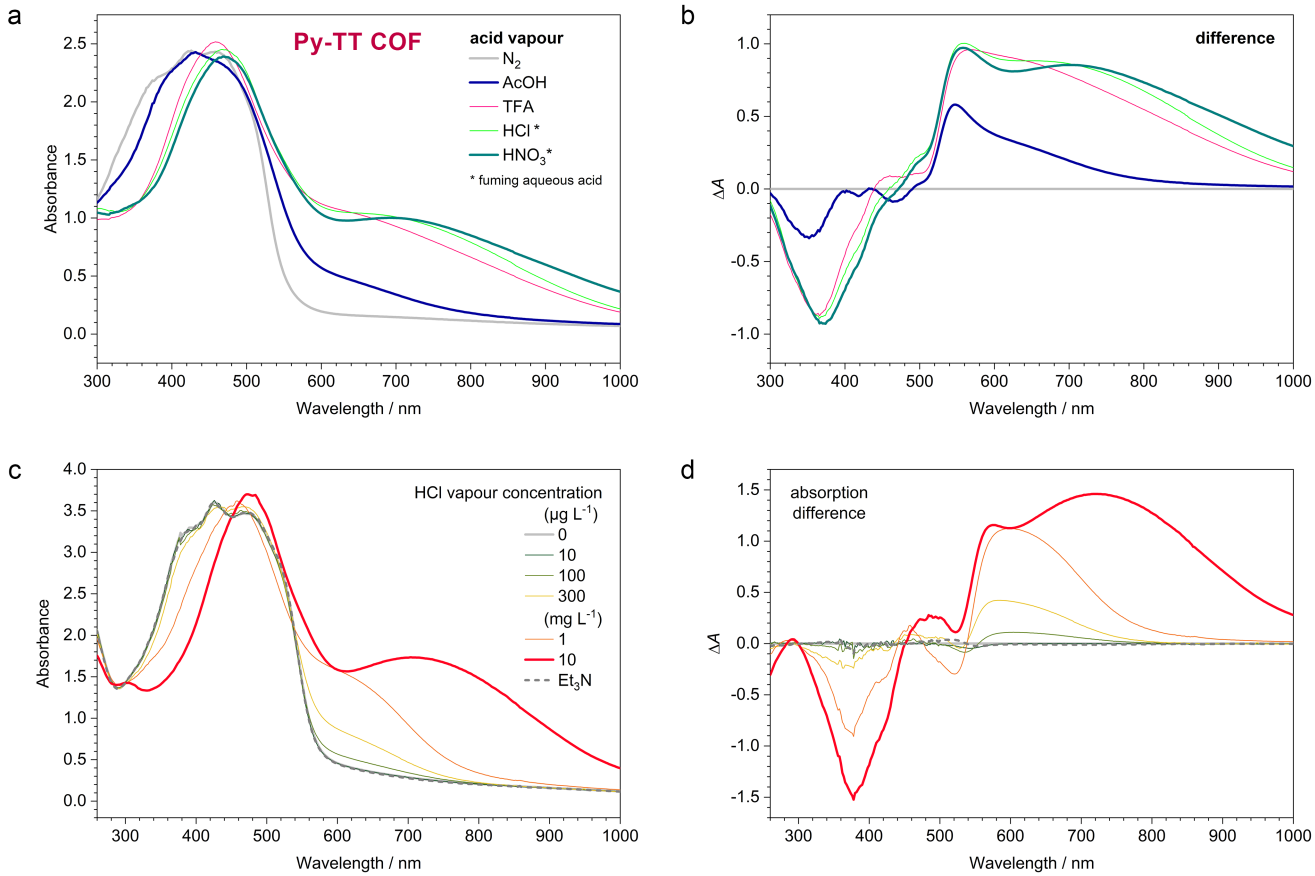

Figure S13. Protonation of a Py-TT COF film with acid vapours. (**a**) Absorption spectra of the COF film in nitrogen and in different acid vapour-saturated atmospheres. (**b**) The corresponding absorption difference spectra. Acetic acid vapour (blue line) generates mainly the mono-protonated COF species, whereas TFA and the strong mineral acids generate predominantly the bis-protonated form. (**c**) HCl vapour sensing using a ca. 350 nm thick Py-TT COF film. The COF combines a very low detection limit of around 100 µg L^{-1} with a response range of at least three orders of magnitude. The detection limit of the COF is more than an order of magnitude below the detection limit of comparable porphyrin-MOF HCl sensors.[11] HCl sensors based on a halide exchange mechanism can reach even lower detection limits,[12] but lack the broad response range. (**d**) Absorption difference between the protonated and the non-protonated COF. While at low acid vapour concentrations the mono-protonated COF is formed predominantly, the spectral signatures of the bis-protonated species become apparent at higher concentrations (orange and red lines).

O. TD-DFT calculations

Time-dependent density functional theory (TD-DFT) calculations were performed on the Py-TT COF fragment displayed below using the ORCA program[13] with the B3LYP hybrid functional[14] and the 6-31G** basis set.

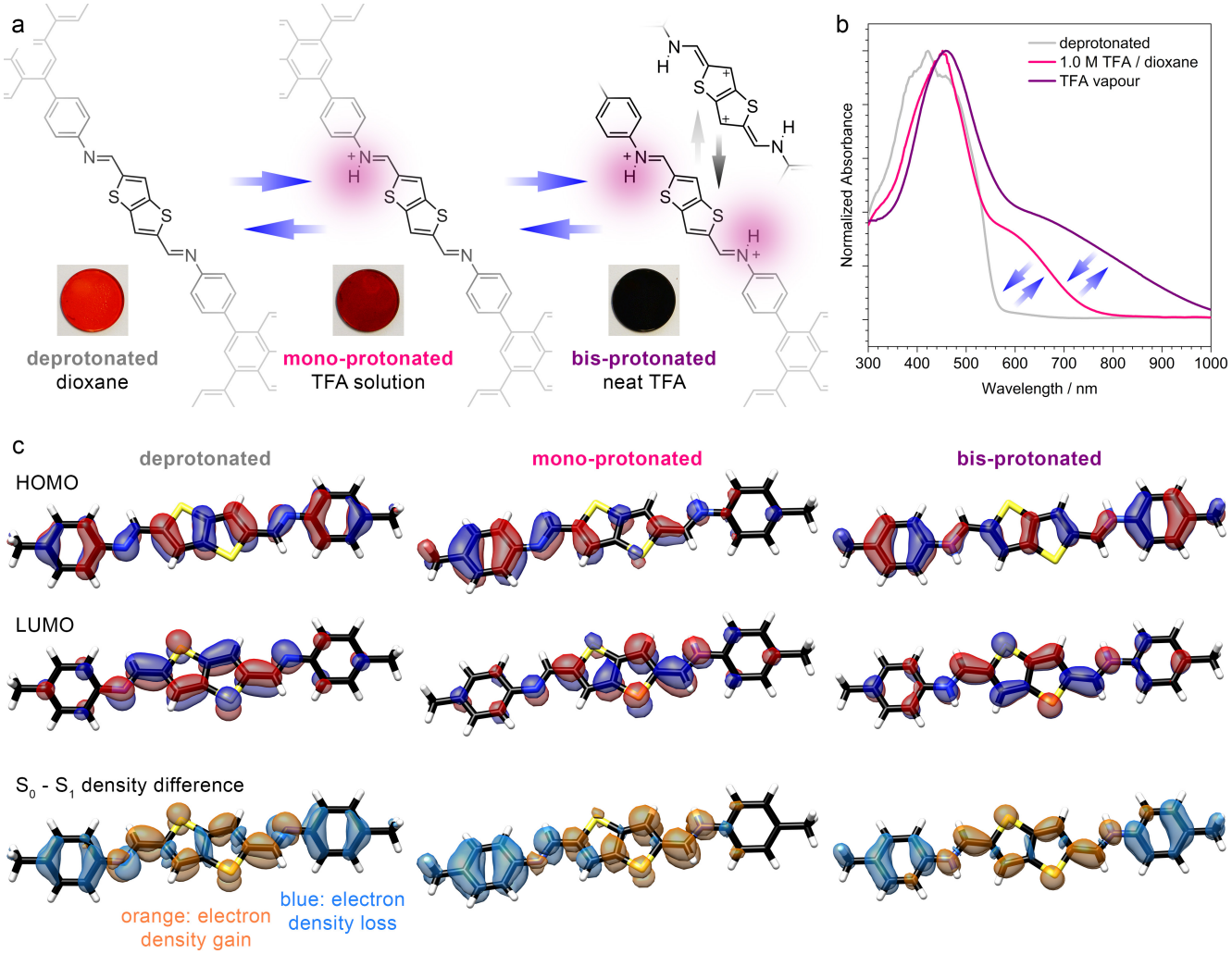

Figure S14. Stepwise protonation of the imine-linked bridges. (**a**) The imine-linked bridges of the Py-TT COF can be protonated in two steps, causing a colour change of the initially orange COF film to brown (mono-protonation, achieved with a 1.0 M TFA solution in 1,4-dioxane) and black (bis-protonation in neat TFA vapour), respectively. TFA = trifluoroacetic acid. The bis-protonated state has a possible quinoidal resonance structure that contributes potentially to the significant red-shift compared to the mono-protonated form. (**b**) Absorption spectra of the non-protonated (grey), mono-protonated (pink) and bis-protonated (purple) Py-TT COF thin films. The spectrum of the bis-protonated COF was recorded using a slightly thinner, but otherwise identical Py-TT COF sample. (**c**) TD-DFT derived frontier orbitals and electron density shifts upon one-electron excitation from the ground state to the first singlet excited state. The model system is a dimethyl-terminated phenylene-imine-thienothiophene-imine-phenylene bridge fragment in the deprotonated (left), mono-protonated (middle), and bis-protonated (right) state. Since the protonated imine is an even stronger acceptor than the free-base imine, the charge-transfer character of the lowest-energy optical transitions increases with the number of protonated imines per bridge. This is accompanied by a successive lowering of the excitation energy, leading to the observed red-shifted absorption. Blue: electron density loss, orange: electron density gain. Wavefunction isosurfaces are displayed with an isovalue of 0.03 $e^{1/2}$ $Bohr^{-3/2}$ and electron density surfaces are displayed with an isovalue of 0.001 e $Bohr^{-3}$.

P. References

1. Düren, T.; Millange, F.; Férey, G.; Walton, K. S.; Snurr, R. Q., Calculating Geometric Surface Areas as a Characterization Tool for Metal-Organic Frameworks. *J. Phys. Chem. C* **2007,** *111*, 15350-15356.

2. Ascherl, L.; Sick, T.; Margraf, J. T.; Lapidus, S. H.; Calik, M.; Hettstedt, C.; Karaghiosoff, K.; Döblinger, M.; Clark, T.; Chapman, K. W.; Auras, F.; Bein, T., Molecular docking sites designed for the generation of highly crystalline covalent organic frameworks. *Nat. Chem.* **2016,** *8*, 310-316.

3. Auras, F.; Ascherl, L.; Hakimioun, A. H.; Margraf, J. T.; Hanusch, F. C.; Reuter, S.; Bessinger, D.; Döblinger, M.; Hettstedt, C.; Karaghiosoff, K.; Herbert, S.; Knochel, P.; Clark, T.; Bein, T., Synchronized Offset Stacking: A Concept for Growing Large-Domain and Highly Crystalline 2D Covalent Organic Frameworks. *J. Am. Chem. Soc.* **2016,** *138*, 16703-16710.

4. Ascherl, L.; Evans, E. W.; Hennemann, M.; Di Nuzzo, D.; Hufnagel, A. G.; Beetz, M.; Friend, R. H.; Clark, T.; Bein, T.; Auras, F., Solvatochromic covalent organic frameworks. *Nat. Commun.* **2018,** *9*, 3802.

5. Chen, X.; Huang, N.; Gao, J.; Xu, H.; Xu, F.; Jiang, D., Towards covalent organic frameworks with predesignable and aligned open docking sites. *Chem. Commun.* **2014,** *50*, 6161-6163.

6. Coventry, D. N.; Batsanov, A. S.; Goeta, A. E.; Howard, J. A. K.; Marder, T. B.; Perutz, R. N., Selective Ir-catalysed borylation of polycyclic aromatic hydrocarbons: structures of naphthalene-2,6-bis(boronate), pyrene-2,7-bis(boronate) and perylene-2,5,8,11-tetra(boronate) esters. *Chem. Commun.* **2005**, 2172-2174.

7. Jin, S.; Sakurai, T.; Kowalczyk, T.; Dalapati, S.; Xu, F.; Wei, H.; Chen, X.; Gao, J.; Seki, S.; Irle, S.; Jiang, D., Two-Dimensional Tetrathiafulvalene Covalent Organic Frameworks: Towards Latticed Conductive Organic Salts. *Chem. Eur. J.* **2014,** *20*, 14608-14613.

8. Keller, N.; Bessinger, D.; Reuter, S.; Calik, M.; Ascherl, L.; Hanusch, F. C.; Auras, F.; Bein, T., Oligothiophene-Bridged Conjugated Covalent Organic Frameworks. *J. Am. Chem. Soc.* **2017,** *139*, 8194-8199.

9. Keller, N.; Calik, M.; Sharapa, D.; Soni, H. R.; Zehetmaier, P. M.; Rager, S.; Auras, F.; Jakowetz, A. C.; Görling, A.; Clark, T.; Bein, T., Enforcing Extended Porphyrin J-Aggregate Stacking in Covalent Organic Frameworks. *J. Am. Chem. Soc.* **2018,** *140*, 16544-16552.

10. Ledbetter, J. W., Infrared Spectra of *N*-Aryl Imines of *o*-Hydroxybenzaldehyde between 2000 and 1500 cm^{-1}. *J. Phys. Chem.* **1977,** *81*, 54-59.

11. Deibert, B. J.; Li, J., A distinct reversible colorimetric and fluorescent low pH response on a water-stable zirconium–porphyrin metal–organic framework. *Chem. Commun.* **2014,** *50*, 9636-9639.

12. Zhao, C.-W.; Ma, J.-P.; Liu, Q.-K.; Wang, X.-R.; Liu, Y.; Yang, J.; Yang, J.-S.; Dong, Y.-B., An in situ self-assembled Cu4I4–MOF-based mixed matrix membrane: a highly sensitive and selective naked-eye sensor for gaseous HCl. *Chem. Commun.* **2016,** *52*, 5238-5241.

13. Neese, F., The ORCA program system. *WIREs Comput. Mol. Sci.* **2012,** *2*, 73-78.

14. Becke, A. D., A new mixing of Hartree-Fock and local density-functional theories. *J. Chem. Phys.* **1993,** *98*, 1372-1377.